

Machine learning-guided construction of an analytic kinetic energy functional for orbital free density functional theory

Sergei Manzhos¹, Johann Lüder² and Manabu Ihara¹

¹ School of Materials and Chemical Technology, Institute of Science Tokyo, Ookayama 2-12-1, Meguro-ku, Tokyo, 152-8552, Japan

² Department of Materials and Optoelectronic Science, National Sun Yat-sen University, 80424, No. 70, Lien-Hai Road, Kaohsiung, Taiwan

E-mail: Manzhos.s.aa@m.titech.ac.jp

Abstract

Machine learning (ML) of kinetic energy functionals (KEF) for orbital-free density functional theory (OF-DFT) holds the promise of addressing an important bottleneck in large-scale *ab initio* materials modeling where sufficiently accurate analytic KEFs are lacking. However, ML models are not as easily handled as analytic expressions; they need to be provided in the form of algorithms and associated data. Here, we bridge the two approaches and construct an analytic expression for a KEF guided by interpretative machine learning of crystal cell-averaged kinetic energy densities ($\bar{\tau}$) of several hundred materials. A previously published dataset including multiple phases of 433 unary, binary, and ternary compounds containing Li, Al, Mg, Si, As, Ga, Sb, Na, Sn, P, and In was used for training, including data at the equilibrium geometry as well as strained structures. A hybrid Gaussian process regression – neural network (GPR-NN) method was used to understand the type of functional dependence of $\bar{\tau}$ on the features which contained cell-averaged terms of the 4th order gradient expansion and the product of the electron density and Kohn-Sham effective potential. Based on this analysis, an analytic model is constructed that can reproduce Kohn-Sham DFT energy-volume curves with sufficient accuracy (pronounced minima that are sufficiently close to the minima of the Kohn-Sham DFT-based curves and with sufficiently close curvatures) to enable structure optimizations and elastic response calculations.

Keywords: orbital-free DFT, kinetic energy functional, Gaussian process regression, additive kernel

1. Introduction

The development of kinetic energy functionals (KEF) for orbital-free (OF) density functional theory (DFT) that would be sufficiently accurate for use in applied modeling of most classes of materials remains an outstanding challenge. Computational materials modeling at the electronic structure level is dominated by Kohn-Sham (KS) DFT [1] whose CPU cost with system size scales formally near-cubically. This severely limits the range of applicability of DFT, whereby KS-

DFT calculations are routinely doable on model systems not exceeding 10^2 to 10^3 atoms in size. This excludes a range of practically important phenomena that are intrinsically large-scale, such as microstructure-driven properties, biomolecular systems, disordered systems, low-concentration doping, etc. [2–4]. The current reliance on force fields for atomistic modeling of respective structures and phenomena is problematic, as force fields present only a crude approximation of the interatomic interactions landscape and cannot model electronic structure and electronic properties

that are needed for mechanistic understanding of large-scale phenomena.

While other approaches to address the scaling issue exist such as order- N DFT [5–9] and semiempirical methods [10–16], they come at a cost of sometimes limiting approximations or parameterizations and at this point still do not address the issue of *routine* large-scale ab initio calculations in substance, as either scaling or the prefactor of the CPU cost remain unfavorable. We stress the need for routine rather than one-off large-scale ab initio calculations, that are needed to screen multiple compositions and structures, perform long time-scale dynamics calculations, etc.

A method possessing the capability of routine (with calculations on systems of 10^5 atoms doable on a desktop within hours) large-scale ab initio calculations *par excellence* is OF-DFT. OF-DFT corresponds to the original formulation of DFT [17] whereby the energy of a system of atoms (atomic cores and electrons) is expressed as a functional of electron density, $E = E[\rho(\mathbf{r})]$. In the absence of accurate functionals of the density, KS DFT [1,18] offered a practical way of computing $E[\rho(\mathbf{r})]$ via one-electron orbitals-solutions of the Kohn-Sham equation $\psi_i(\mathbf{r})$:

$$\begin{aligned}
E[\rho(\mathbf{r})] &= -\frac{1}{2} \sum_{i=1}^{N_{el}} \int \psi_i^*(\mathbf{r}) \nabla^2 \psi_i(\mathbf{r}) d\mathbf{r} \\
&\quad + \frac{1}{2} \iint \frac{\rho(\mathbf{r}')\rho(\mathbf{r})}{|\mathbf{r} - \mathbf{r}'|} d\mathbf{r} d\mathbf{r}' \\
&\quad + \int V_{ion}(\mathbf{r})\rho(\mathbf{r}) d\mathbf{r} + E_{XC}[\rho(\mathbf{r})] \\
&\equiv E_{kin}[\{\psi_k(\mathbf{r})\}] + E_H[\rho(\mathbf{r})] + E_{ion}[\rho(\mathbf{r})] \\
&\quad + E_{XC}[\rho(\mathbf{r})] \\
\rho(\mathbf{r}) &= \sum_{i=1}^{N_{el}} |\psi_i(\mathbf{r})|^2 d\mathbf{r}
\end{aligned} \tag{1}$$

Unless stated otherwise, we use atomic units. N_{el} is the number of electron pairs (we neglected spin and partial occupancy without loss of generality of the present discussion). $E_H[\rho(\mathbf{r})]$ is the Hartree energy (due to Coulombic interactions within the electron density), $E_{ion}[\rho(\mathbf{r})]$ is the energy due to Coulombic interactions of the electron density and the Coulombic potential due to ionic cores and any additional external electric fields, and $E_{XC}[\rho(\mathbf{r})]$ is the exchange-correlation (XC) term that ensures that the electron density and the total energy computed from the orbitals match those of the system computed with the full many-body electronic wavefunction. The integrals are over the extent of the system (i.e. over the periodic cell for periodic systems or all space for non-periodic systems). $E_{kin}[\{\psi_k(\mathbf{r})\}]$ is the kinetic energy dependent on the entire set $\{\psi_k(\mathbf{r})\}$ of occupied orbitals. It is only E_{kin} that requires the calculation of orbitals for eq. (1), all other terms can be computed directly

as functionals of the density. The orbitals are also used for the calculation and analysis of band structure and excitations. The formally cubic scaling of DFT comes from the need to compute the orbitals (to solve the Kohn-Sham equation).

Over decades, a range of exchange-correlation functionals were developed providing accuracies of structures, bandstructures, excitation energies, etc. sufficiently high for their use in applied modelling (i.e. possessing predictive power) of all major classes of materials: organic and inorganic, semiconducting and metallic, periodic and non-periodic. It could be said that the key bottleneck has shifted from the accuracy of DFT to its ability to compute larger, and therefore more realistic, systems. OF-DFT addresses this bottleneck by using a kinetic energy functional (KEF) of the electron density computed without recourse to the orbitals,

$$E_{kin}[\rho(\mathbf{r})] = \int \tau(\mathbf{r}) d\mathbf{r} \tag{2}$$

where $\tau(\mathbf{r})$ is kinetic energy density (KED). $E[\rho(\mathbf{r})]$ can then be computed with linear scaling and a small prefactor, and the bottleneck shift to the accuracy of the KEF. One can rely on existing XC functionals and aim at a KEF reproducing KS kinetic energy or KS KED,

$$\begin{aligned}
E_{kin}[\rho(\mathbf{r})] &= \frac{1}{2} \sum_{i=1}^{N_{el}} \int \psi_i^*(\mathbf{r}) \nabla^2 \psi_i(\mathbf{r}) d\mathbf{r} \equiv \int \tau_{KS}(\mathbf{r}) d\mathbf{r} \\
&= \int \tau_{KS}^+(\mathbf{r}) d\mathbf{r}
\end{aligned} \tag{3}$$

where $\tau_{KS}(\mathbf{r}) = \frac{1}{2} \sum_{i=1}^{N_{el}} \psi_i^*(\mathbf{r}) \nabla^2 \psi_i(\mathbf{r})$ and $\tau_{KS}^+(\mathbf{r}) = \frac{1}{2} \sum_{i=1}^{N_{el}} |\nabla \psi_i(\mathbf{r})|^2$ are Kohn-Sham KED and its positively-definite version (integrating to the same kinetic energy), respectively.

Existing analytic approximations for $E_{kin}[\rho(\mathbf{r})]$ already provide KS-DFT-like accuracy for light metals [19–26]. For other classes of materials, major issues remain, including the ability to correctly model potential energy surfaces - a prerequisite for structure optimization without which the method cannot be used in most applications. In recent years, there have been substantial developments enabling mechanistic analyses and calculations of optical spectra without recourse to orbitals [27–33]. Progress has also been made in the development of OF-DFT-suited pseudopotentials [34–37], including with the help of machine learning (ML) [22,38,39]. Several OF-DFT-capable codes are available where new KEFs can be eventually implemented [31,40–43]. The onus thus shifts to building good KEF models for different classes of materials including metals, semiconductors, and molecular materials. While steady progress is being made [30,44–49], improvements are needed. In the absence of a universal $E_{kin}[\rho(\mathbf{r})]$, widespread use of OF-DFT applications

can succeed as sufficiently accurate $E_{kin}[\rho(\mathbf{r})]$ approximations are built for specific materials classes and or applications, similar to the state of KS DFT where a plethora of XC functionals are currently used for different applications.

Renewed interest in OF-DFT and specifically KEF research has been spurred in recent years by the possibility of machine-learning the $E_{kin}[\rho(\mathbf{r})]$ [50–64]. Most works, including those of the present authors [51–53,62], machine-learned KS KED from density-dependent features that typically include derivatives and powers of the electron density. When using the terms of the 4th order gradient expansion [65]

$$\tau_{GE4}(\mathbf{r}) = \tau_{TF}(\mathbf{r}) \left(1 + \frac{5}{27}p(\mathbf{r}) + \frac{20}{9}q(\mathbf{r}) + \frac{8}{81}q(\mathbf{r})^2 - \frac{1}{9}p(\mathbf{r})q(\mathbf{r}) + \frac{8}{243}p(\mathbf{r})^2 \right) \quad (4)$$

where $\tau_{TF}(\mathbf{r})$ is the Thomas-Fermi KED [66], and $p(\mathbf{r}) = \frac{|\nabla\rho(\mathbf{r})|^2}{4(3\pi^2)^{2/3}\rho(\mathbf{r})^{8/3}}$ and $q(\mathbf{r}) = \frac{\Delta\rho(\mathbf{r})}{4(3\pi^2)^{2/3}\rho(\mathbf{r})^{5/3}}$ are the squared gradient and scaled Laplacian of the density, respectively, as well as the product of the electron density and Kohn-Sham effective potential $\rho(\mathbf{r})v_{eff}(\mathbf{r})$ as features, we were able to reproduce energy-volume curves of several materials simultaneously with an ML model based on kernel regression [52,62].

One disadvantage of ML of $\tau_{KS}(\mathbf{r})$ is the need to wield large data sets, with each structure of a material contributing possibly millions of data points. For example, sampling $\tau_{KS}(\mathbf{r})$ of Li, Al, and Si on their respective Fourier grids (of plane wave reference DFT calculations) resulted in about 600,000 datapoints [52,62]. This makes growing the training set to achieve a more portable KEF difficult, especially for materials with larger unit cells. Another challenge is the very uneven distribution of $\tau_{KS}(\mathbf{r})$ and of terms of eq. (4) which complicates ML [51,52,62]. In Ref. [62], this was addressed by smoothing $\tau_{KS}(\mathbf{r})$ and the features, which allowed accurate ML with relatively few training points. Fully averaging (over the simulation cell) would make each material structure contribute a single point to the training set. While this can inhibit machine learning from a smaller number of structures, when the number of materials in the training set is large enough, this is advantageous, as was done in Ref. [67] when machine-learning crystal cell-averaged KED ($\bar{\tau}$) of 433 unary, binary, and ternary compounds containing Li, Al, Mg, Si, As, Ga, Sb, Na, Sn, P, and In, including data at the equilibrium geometry as well as strained structures. Machine-learning cell-averaged KED rather than the integrated E_{kin} is advantageous as it palliates the issue of different materials having different crystal cell sizes. In this work, we also machine learn $\bar{\tau}$ from the same data as in Ref. [67].

Another disadvantage of ML models of a KEF is that they are not as easily handled as analytic expressions can be. They

need to be provided in the form of algorithms and associated data, as was done for example in Refs. [67,68]. This causes additional complexity, compared to an analytic formula, of integrating the model into various codes and of analytic manipulations important for theory development. The black-box nature of generic ML methods such as neural networks, kernel regression, and gradient boosted decision trees to which the problem of machine learning a KEF is amenable also typically means lack of insight. Domain knowledge-specific ML methods are possible [69–72], but they lose one of the appeals of black-box ML methods which is precisely their generic nature.

Here, we build an analytic model of a kinetic energy functional, guided by a machine learning algorithm. We use the hybrid Gaussian process regression – neural network (GPR-NN) method [73] which, while fully general, allows for the analysis of the type of functional dependence of the target on the features, including the roles of nonlinearity and inter-feature coupling. GPR-NN was used previously for insightful ML in materials informatics and other applications [74–79]. Here, we use it to derive an analytic model of a KEF that is able to reproduce Kohn-Sham DFT energy-volume curves with good accuracy.

2. Methods and data

2.2 Data

We use the dataset provided in Ref. [67] that includes the crystal cell-averaged KED $\bar{\tau}$ (the target) and crystal cell-averaged terms of the 4th order gradient expansion as well as crystal cell-averaged product of the electron density and Kohn-Sham effective potential, forming a six-dimensional feature vector $\mathbf{x} = (\bar{\tau}_{TF}, \overline{\tau_{TF}p}, \overline{\tau_{TF}p^2}, \overline{\tau_{TF}pq}, \overline{\tau_{TF}q^2}, \overline{\rho v_{eff}})$. The term $\tau_{TF}q(\mathbf{r})$ is not used as it averages to zero. The data are computed with plane wave KS DFT and local pseudopotentials in Abinit [80], using the PBE functional [81]. It is computed for 433 unary, binary, and ternary compounds containing Li, Al, Mg, Si, As, Ga, Sb, Na, Sn, P, and In, including data at the equilibrium geometry as well as strained structures (18 structures for each composition, including the equilibrium structure as well as isotropically strained structures ranging from $0.93V_0$ to $1.10V_0$, where V_0 is the equilibrium volume), for a total of 7794 data points. See Ref. [67] for other computational details. The features were scaled on the unit cube unless indicated otherwise. 80% of the data were used for training and 20% for testing unless otherwise indicated. We confirmed that there is no significant difference between different random training-test splits; we therefore fix the random seed in the following to facilitate comparisons.

2.2 Machine learning

We use the GPR-NN method of Ref. [73] which is effectively a hybrid between a single-hidden layer NN and GPR. A target function $f(\mathbf{x}), \mathbf{x} \in R^D$ (which in this case is $\bar{\tau}(\mathbf{x}), \mathbf{x} \in R^6$) is represented as a first-order additive model in redundant coordinates $\mathbf{y} \in R^N, N > D$:

$$f(\mathbf{x}) = \sum_{n=1}^N f_n(y_n) \quad (5)$$

where the component functions $f_n(y_n)$ are built with GPR

$$f_n(y_n) = \sum_{k=1}^M a_{nk} k(y_n, y_n^{(k)}) \quad (6)$$

where $k(y_n, y_n^{(k)})$ is the kernel and k indexes training data points. The kernel is one-dimensional and therefore issues with high-dimensional kernels [79,82,83] are avoided. We use the square exponential kernel, i.e. $k(y, y') = \exp(-(y - y')^2 / 2l^2)$. The redundant coordinates y_n are linear functions of $\mathbf{x}, \mathbf{y} = \mathbf{W}\mathbf{x}$, where \mathbf{W} is defined by rules and is not optimized. Here, the original coordinates \mathbf{x} are included as a subset of \mathbf{y} ($y_n = x_n$ for $n = 1, \dots, D$) and the rows of matrix \mathbf{W} defining other y_n are chosen as elements of a D -dimensional Sobol sequence [84]. All terms $f_n(y_n)$ of eq. (5) are computed as a single linear step with a standard GPR code where one defines an additive kernel in \mathbf{y} [85,86]. The only CPU cost overhead vs. standard GPR is the summation in the kernel. Functions $f_n(y_n)$ are optimal in the least squares sense for given \mathbf{W} and data.

Eq. (5) is equivalent to a single-hidden layer NN with N neurons, a linear output neuron, and optimal shapes of neuron activation functions for each neuron. It possesses therefore a universal approximator property [87–101]. Note that biases and output weights are subsumed in the definition of $f_n(y_n)$ and need not be considered separately. As no nonlinear optimization is done, the method is as robust as linear regression (as GPR is a regularized linear regression with nonlinear basis functions derived from the kernel function [79,102]), and there is no overfitting as N exceed the optimal number of neurons [73].

Control of N allows studying importance of features, functional dependency of the target on features, and importance of coupling [74,75,79]. Here, we use this capability of the method to build an analytic model of a KEF based on machine learning results.

Calculations are performed in Matlab R2022b. The code for the GPR-NN method is provided in Ref. [73]. The version of the code modified for the present application can be obtained from the authors. Hyperparameters are selected by grid search. Optimal values were around $l = 0.5$ for the length parameter of the (isotropic in \mathbf{y}) kernel and $\log \sigma = -5$ for the logarithm

of the noise parameter. While there are slight variations in the optimal values with N , they are not significant, so that the hyperparameters were fixed at these values.

The quality of energy-volume curves was estimated by the error in the quantity characterizing the curvature of the energy volume curve at its minimum,

$$B = V_0^2 \frac{d^2 E}{dV^2} \approx B' = \frac{E(V_0 - \Delta V) - 2E(V_0) + E(V_0 + \Delta V)}{(\Delta V/V_0)^2} \quad (7)$$

where V_0 is the equilibrium volume, $\Delta V/V_0 = 3\%$, and E the total energy. The total energy with the ML KEF model was estimated by subtracting KS kinetic energy from KS DFT total energy and replacing it with model-predicted kinetic energy (which is the product of $\bar{\tau}$ and the volume).

3. Results

We first fitted $\bar{\tau}(\mathbf{x})$ with GPR-NN for different N to understand obtainable accuracy with the method vs. previous calculations on the data. In Ref. [67], the best GPR model of that work obtained an RMSE (root mean square error) in $\bar{\tau}$ of 1.05×10^{-5} and 1.47×10^{-5} a.u. for the training and test sets, respectively. This corresponded in the error in B' of 13% in terms of MRE (mean absolute relative error) and 8% in terms of MDRE (median absolute relative error), and energy-volume curves of the vast majority of the 433 materials sufficiently close to KS DFT computed curves to result in meaningful structure optimization, stiffness calculations, etc. To achieve such accuracy, correlation coefficients R between reference and model-predicted $\bar{\tau}$ had to exceed 0.99999 (“five nines”). To compare, linear regression resulted in RMSE in $\bar{\tau}$ of about 4×10^{-5} a.u. (for both the training and test sets), MRE and MDRE of about 55% and 25%, respectively, and energy-volume curves of many materials that did not exhibit a minimum around the equilibrium geometry. This even though R of about 0.9999 (“four nines”) was high by the standards of most ML applications. This highlights that ML for KEF development required extremely accurate ML. This is of course not surprising as interaction energies defining energy-structure dependence are small compared to the total energy.

In Table 1, we summarize accuracy achievable with GPR-NN with different numbers of terms N . Note that $N = 6$ corresponds to a simple additive model in \mathbf{x} ($\mathbf{y} = \mathbf{x}$). Key observations from these results are

(i) GPR-NN achieves an accuracy competitive with full-dimensional GPR already with an additive model. While levels of RMSE in $\bar{\tau}$ are a tad higher than with GPR, the accuracy of B' is similar and is slightly better. The correlation coefficient approaching “five nines” is obtained.

(ii) increasing N i.e. adding coupling terms, further decreases RMSE in $\bar{\tau}$ to better levels than was achieved with GPR, R is also increased beyond “five nines”, but with limited additional benefit to the quality of the energy volume curves

exemplified by MRE and MDRE of B' values. This is not surprising, as the ML algorithm only aims to improve the aggregate error in $\bar{\tau}$, while the errors in B' , that are essentially interaction energy errors, are influenced by any error cancellations or accumulation.

We therefore take a closer look at the additive model corresponding to $N = 6$. We manually adjust the scaling of

some coordinates thus introducing an effect that an anisotropic kernel would have while keeping the kernel isotropic. The results are given in the table under “6’”. The fit quality is slightly worse but allows obtaining slightly better low-order polynomial fits below.

Table 1. Errors in $\bar{\tau}$ and in B' achieved with GPR-NN with different numbers of terms N . $N = 6$ corresponds to first-order additive model in \mathbf{x} . Also given is the correlation coefficient R between Kohn-Sham and predicted $\bar{\tau}$ values.

N	Error in $\bar{\tau}$, $\times 10^5$ a.u.		Error in B' , %		R , digits xxx in 0.9999xxx	
	training	test	MRE	MDRE	train	test
6	1.81	1.87	10.5	6.4	863	844
6'	1.87	1.91	10.9	7.5	853	837
20	1.35	1.38	10.3	6.8	924	915
50	1.21	1.23	10.6	8.0	939	932
100	1.15	1.16	10.6	7.9	945	939

Figure 1 shows the correlation plot between the exact (Kohn-Sham DFT-based) and ML model-predicted $\bar{\tau}$ from the additive model ($\mathbf{y} = \mathbf{x}$) for the model corresponding to “6’” in Table 1 as well as the importance of component functions by the square root of their variance. The correlation plot is practically linear; we show it here just to highlight the level of accuracy required in this application vs mainstream ML applications such as e.g. materials informatics or ML force fields. The plot of relative importance of features indicates the following:

(i) a large fraction of the variance of the target is captured by $\overline{p v_{eff}}$. This is expected, because the KS KED can be expressed as $\tau_{KS}(\mathbf{r}) = \sum_i \epsilon_i |\psi_i(\mathbf{r})|^2 - v_{eff}(\mathbf{r}) \rho(\mathbf{r})$, where ϵ_i are Kohn-Sham eigenvalues.

(ii) all features have important contributions. Indeed, we confirmed by doing calculations with some features removed from the set that a good accuracy cannot be obtained unless all of them are included.

(iii) comparing feature importance vs. the gradient expansion, we observe that the model assigns a weight to the von Weizsäcker-dependent term which is about 0.133 of that of the Thomas-Fermi-dependent term, which is somewhat smaller than gradient expansion’s $5/27$ but is of the same order. The relative magnitudes of the $\overline{\tau_{TF} p^2}$, $\overline{\tau_{TF} p q}$, $\overline{\tau_{TF} q^2}$ terms vs the TF term (about 0.152, 0.233, and 0.214, respectively) are somewhat larger than in the gradient expansion. The fact that the ML model returns physically meaningful relative magnitudes is to note. Importantly, the gradient expansion is *linear* in x_1, \dots, x_5 , while the ML model is *nonlinear*.

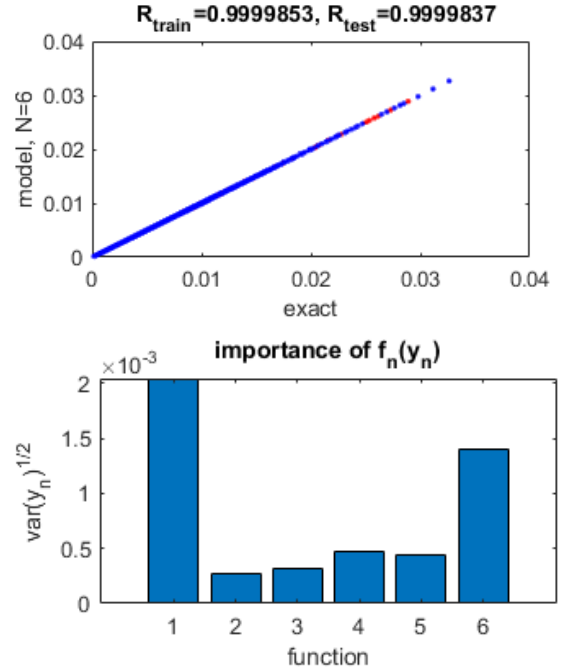


Figure 1. Top panel: the correlation plot between the exact (Kohn-Sham DFT-based) and model-predicted crystal cell-averaged kinetic energy density $\bar{\tau}$ from the additive model ($\mathbf{y} = \mathbf{x}$). The model corresponds to “6’” in Table 1. Blue points are from the training and red points from the test set (many are invisible due to the high quality of the fit). Corresponding correlation coefficients are shown on top of the plot. Bottom panel: the importance of component functions by the square root of their variance Numbers on the abscissa index n .

Nonlinearity is critically important: we can force the model to be linear by using a very large kernel length parameter [75,82]. For example, with $l = 1000$, $\log \sigma = -10$ (when the

component functions are practically linear), we obtain values of MRE and MDRE in B' of about 38 and 21%, respectively, and RMSE in $\bar{\tau}$ of about 4×10^{-5} a.u. (comparable to results obtained in Ref. [67] with linear regression).

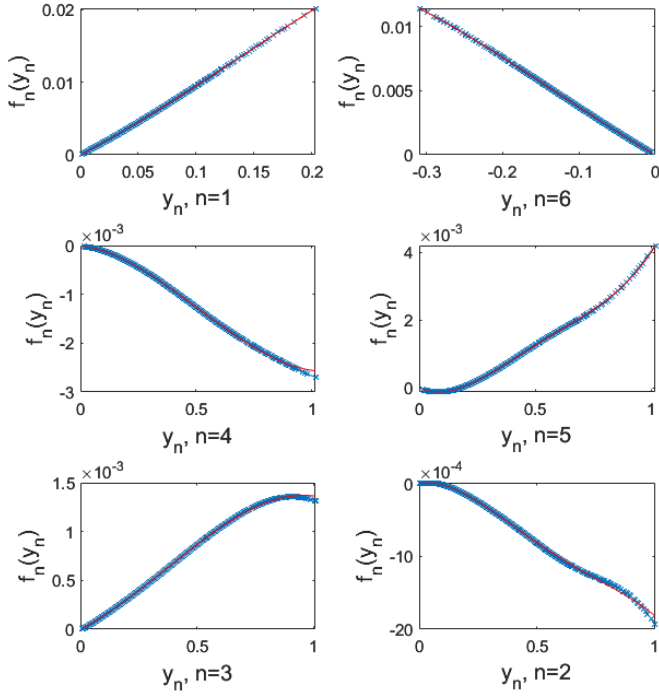


Figure 2. The shapes of the component functions $f_n(y_n)$, in the order of importance (left to right and top to bottom) predicted by the additive model ($\mathbf{y} = \mathbf{x}$). The symbols are the values at the training data points and the red line is the polynomial fit.

$$\begin{pmatrix} 0.082926586827897 & 0.157677447591406 & -0.378760872909400 & 0 \\ 0.000634147249392 & -0.009076865906296 & 0.011656254814405 & -0.005025491981521 \\ 0.001196170711360 & 0.001986140118683 & -0.001816638030194 & 0 \\ -0.000570356598613 & -0.005784298540582 & 0.003797894548784 & 0 \\ -0.003230090903822 & 0.023009315178709 & -0.030436676933612 & 0.014654972864815 \\ -0.035134852665972 & 0.027869731148558 & 0.062744904623325 & -0.029165231906284 \end{pmatrix} \quad (9)$$

In Figure 3 - Figure 6, we show the energy-volume curves computed with KS DFT (blue lines) and the analytic model (red lines) for the entire set of 433 materials (in the same order as they are provided in the dataset of Ref. [67] i.e. by increasing materialsproject (mp) ID which is also shown on the plots). On each graphic, we indicate, besides the chemical formula, the values of B' from KS DFT and model-predicted curves, in respective colors. For the vast majority of the materials, the ML-inspired analytic model results in pronounced minima that are sufficiently close to the minima of the KS DFT curves, and with sufficiently close curvatures to perform structure optimizations and elastic response calculations.

Figure 2 shows the shapes of the component functions. One can appreciate their nonlinear nature. On the other hand, they are sufficiently smooth to be potentially expressible with simple analytic functions.

We therefore fit them with low order polynomials (using all data points). The red line in Figure 2 shows the polynomial fit with 3rd order polynomials for x_1, x_3, x_4 and 4th order polynomials for x_2, x_5, x_6 . Using lower-order polynomials resulted in significant deterioration of the accuracy. The energy volume curves are computed based on the polynomial model. The best polynomial model is obtained with slightly different hyperparameters ($l = 0.35$, $\log \sigma = -4$). The polynomial model obtained RMSE in $\bar{\tau}$ of 2.21×10^{-5} a.u. and MRE and MDRE in B' of 13.6% and 9.5%, respectively. These values are somewhat worse than those achievable with the GPR-NN models but they are by and large similar to those achieved in Ref. [67] with GPR, except that now we can express the KEF as an analytical formula that can be communicated and handled as such. That formula is:

$$\bar{\tau} = \sum_{n=1}^6 \sum_{p=1}^{P_n} a_{np} (x'_n)^p \quad (8)$$

where $\mathbf{P} = (3, 4, 3, 3, 4, 4)$, $\mathbf{x}' = (6.6\overline{\tau_{TF}}, 271\overline{\tau_{TF}p}, 797\overline{\tau_{TF}p^2}, 655\overline{\tau_{TF}pq}, 194\overline{\tau_{TF}q^2}, 8.4\overline{\rho v_{eff}})$, and matrix \mathbf{a} with elements a_{np} is

Overall, the results are not worse than those of a full GPR model (see energy-volume curves of Ref. [67]). Some of the few materials with unfavorable energy volume curves already were so in the GPR model of Ref. [67]. These cases can be seen in, for instance, cubic phases of P and As including mp-10 and mp-53, mp-7245 or the layered AsP (mp-1228795) structure. Those are materials with covalent bonds but in geometries quite different from their ground state, i.e., phases with relatively high energies above hull. Since the calculations generating the database were performed with DFT and local pseudopotentials, a contributing factor could be a limited transferability of the local pseudopotentials of elements like As and P forming covalent bonds. Hexagonal packed Si (mp-

34), or tetragonal phases containing As or P such as mp-130, mp-8882 (GaP) or mp-570744 (Si_3As_4) further support this. Indeed, the ratio of obtaining well matched B' values is, for instance, about 2 times higher for phases containing Mg or 10 times for Sn than for P or Si. Difficulties of the model with layered systems arise from the averaging step that similarly affects structures with void regions such as mp-1072544, a Si phase. Another set of struggling energy volume curves can be seen in Na and Li containing materials where the DFT and GPR-NN curves have noticeable shifts, which could stem from the lack of (semi-) core electrons in the local pseudopotential [103]. Essentially, the ability of the ML model to reproduce the physics with energy volume curves of a broad variety of materials seems to be limited by the restrictions in the data stemming from the local pseudopotential KS DFT calculations, emphasizing the need for comprehensive approaches to simultaneously develop KEF and local pseudopotentials, or rely on all-electron approaches.

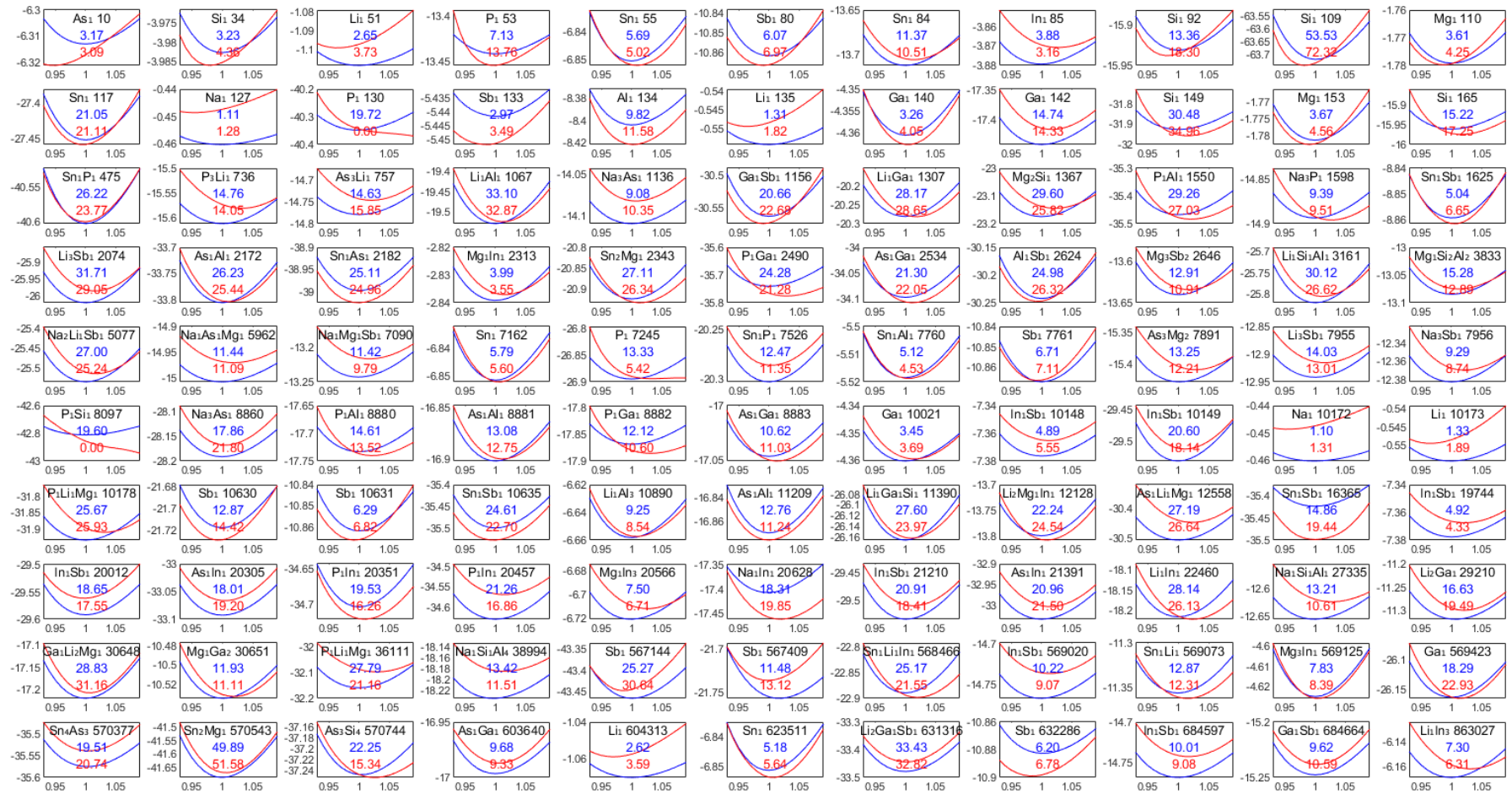


Figure 3. Energy-volume curves for the materials in the dataset. Chemical formula is followed by materialsproject ID. Blue: Kohn-Sham DFT; red: analytic model of $\bar{\epsilon}$. The abscissa values are V/V_0 with the equilibrium volume at $V/V_0 = 1$, and the ordinate axis is total energy in a.u. The values of B' from KS DFT and model-predicted curves are shown blue and red, respectively.

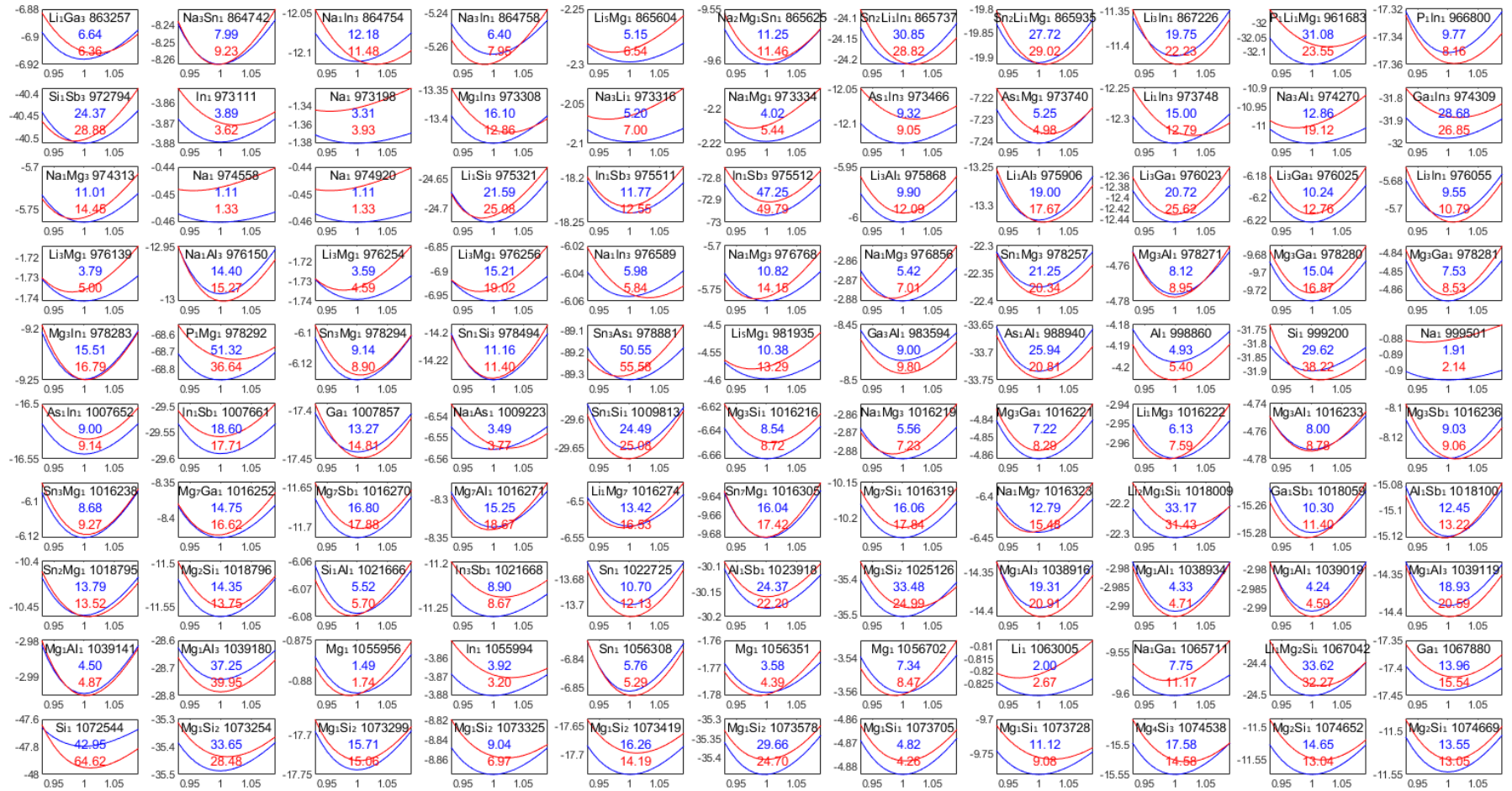


Figure 4. Energy-volume curves for the materials in the dataset (continued). Chemical formula is followed by materialsproject ID. Blue: Kohn-Sham DFT; red: analytic model of $\bar{\tau}$. The abscissa values are V/V_0 with the equilibrium volume at $V/V_0 = 1$, and the ordinate axis is total energy in a.u. The values of B' from KS DFT and model-predicted curves are shown blue and red, respectively.

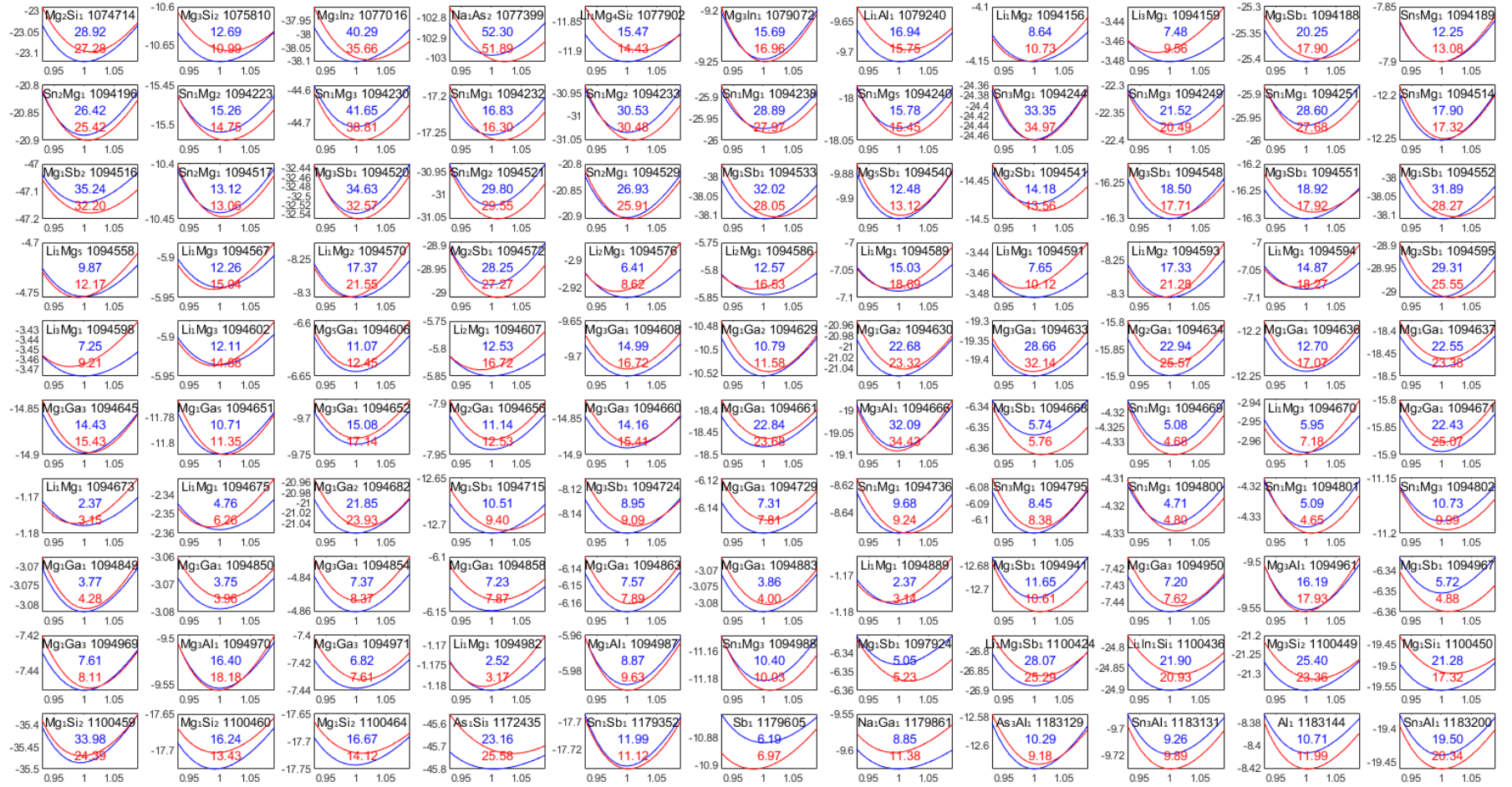


Figure 5. Energy-volume curves for the materials in the dataset (continued). Chemical formula is followed by materialsproject ID. Blue: Kohn-Sham DFT; red: analytic model of $\bar{\tau}$. The abscissa values are V/V_0 with the equilibrium volume at $V/V_0 = 1$, and the ordinate axis is total energy in a.u. The values of B' from KS DFT and model-predicted curves are shown blue and red, respectively.

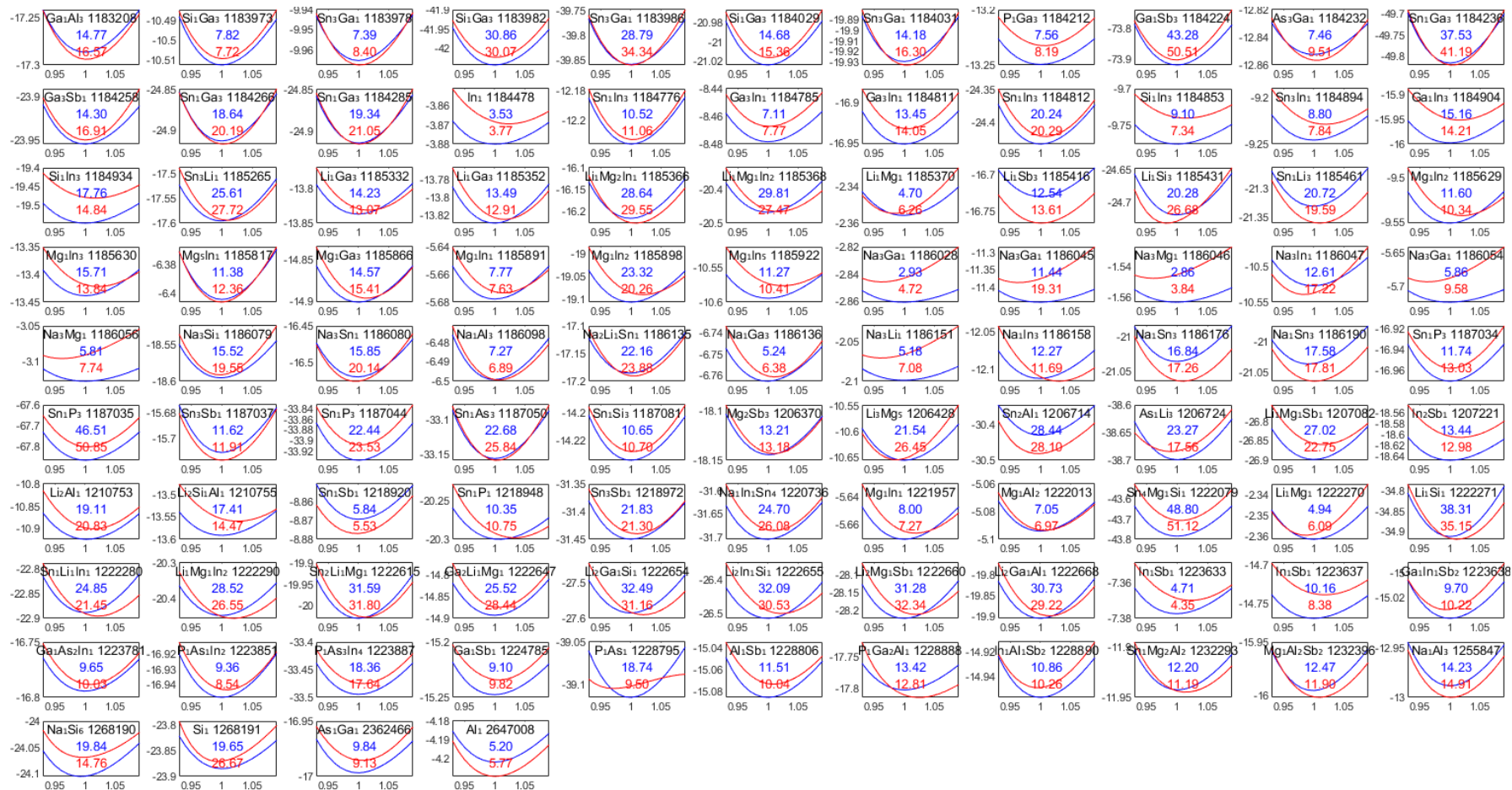


Figure 6. Energy-volume curves for the materials in the dataset (continued). Chemical formula is followed by materialsproject ID. Blue: Kohn-Sham DFT; red: analytic model of $\bar{\tau}$. The abscissa values are V/V_0 with the equilibrium volume at $V/V_0 = 1$, and the ordinate axis is total energy in a.u. The values of B' from KS DFT and model-predicted curves are shown blue and red, respectively.

In principle, any ML model (NN, GPR, or GPR-NN) is expressible analytically (see eqs. (5-6), for example), but such expressions are unwieldy. In the case of GPR, for example, the number of summands is equal to the training data set size; and additional summation in the additive kernel further complicates the expression [104]. In the case of a NN, one sums over multiple layers, multiple neurons per layer, and over terms in the argument of neuron activation functions [105,106]. Such expressions cannot be manipulated as analytic formulas in most practically relevant applications. Equations (8-9) can be.

4. Conclusions

We used machine learning of crystal cell-averaged kinetic energy density to guide the construction of an analytic expression for a kinetic energy functional. We applied the GPR-NN method to the previously published dataset of 433 unary, binary, and ternary compounds containing Li, Al, Mg, Si, As, Ga, Sb, Na, Sn, P, and In [67]. Terms of the 4th order gradient expansion and the product of the electron density and Kohn-Sham effective potential that were used as ML features. GPR-NN, which is a hybrid between neural network and GPR, was able to produce fits of similar or better accuracy than previously reported GPR fits of the same data. Importantly, the use GPR-NN allowed insight into the relative importance of nonlinearity and inter-feature coupling and the shape of functional dependence of the target on the features. The quality of the ML model was evaluated by the quality of the energy-volume curves and the curvature at the minimum of the curve, thus directly addressing the issue of reproducing the topology of the interaction energy which remains a major issue in OF-DFT.

Based on the analysis of GPR-NN results, we constructed a relatively simple analytic expression that is practically as accurate as the best ML model. For most materials, it can reproduce Kohn-Sham DFT energy-volume curves with sufficient accuracy (pronounced minima that are sufficiently close to the minima of the Kohn-Sham DFT-based curves and with sufficiently close curvatures) to enable structure optimizations and elastic response calculations.

ML KEF models are actively pursued for their promise to facilitate large-scale *ab initio* materials modeling with OF-DFT, but they cannot be as easily manipulated (shared, used, analyzed) as analytic formulas - they have to be shared as codes and datasets. Our results effectively bridge the two tracks of KEF development. We hope that they will be informative for future ML applications including OF-DFT functional development for electronic problems and beyond [107], XC functional development [56,108–112] and other ML applications broadly.

Data availability statement

The data used in the manuscript are provided in Ref. [67]. The code for the GPR-NN method is provided in Ref. [73]. A version of the code used specifically in this manuscript is available from the authors.

Acknowledgements

S. M. and M. I. thank JST Mirai Program (grant No. JPMJMI22H1).

J. L. thanks the National Science and Technology Council (NSTC) for financial support under Grant N. 110-2112-M-110-025, and the National Center for High-performance Computing (NCHC) of National Applied Research Laboratories (NARLabs) in Taiwan for providing computational and storage resources.

Author contributions

S. M.: conceptualization (lead); methodology (lead); software (lead); investigation (lead); writing - original draft (lead); writing - review and editing (lead).

J. L.: data curation (lead); investigation (supporting); writing - review and editing (supporting).

M. I.: writing - review and editing (supporting); resources.

Conflicts of interest

The authors declare no competing interests.

References

- [1] Kohn W and Sham L J 1965 Self-Consistent Equations Including Exchange and Correlation Effects *Phys. Rev.* **140** A1133–8
- [2] Okamoto T, Sorkin A, Kameda K, Ihara M, Wang H and Manzhos S 2024 Natural-like generation of grain boundary models and the combined effects of microstructural elements and lithiation on the plastic behavior of TiO₂: A computational study *Computational Materials Science* **239** 112989
- [3] Liu W, Sk M A, Manzhos S, Martin-Bragado I, Benistant F and Cheong S A 2017 Grown-in beryllium diffusion in indium gallium arsenide: An *ab initio*, continuum theory and kinetic Monte Carlo study *Acta Materialia* **125** 455–64
- [4] Li W, Kotsis K and Manzhos S 2016 Comparative density functional theory and density functional tight binding study of arginine and arginine-rich cell penetrating peptide TAT adsorption on anatase TiO₂ *Phys. Chem. Chem. Phys.* **18** 19902–17
- [5] Soler J M, Artacho E, Gale J D, García A, Junquera J, Ordejón P and Sánchez-Portal D 2002 The SIESTA method for *ab initio* order-N materials simulation *J. Phys.: Condens. Matter* **14** 2745–79
- [6] Mohr S, Ratcliff L E, Genovese L, Caliste D, Boulanger P, Goedecker S and Deutsch T 2015 Accurate and efficient linear scaling DFT calculations with universal applicability *Phys. Chem. Chem. Phys.* **17** 31360–70
- [7] Nakata A, Baker J S, Mujahed S Y, Poulton J T L, Arapan S, Lin J, Raza Z, Yadav S, Truflandier L, Miyazaki T and Bowler

- D R 2020 Large scale and linear scaling DFT with the CONQUEST code *J. Chem. Phys.* **152** 164112
- [8] Bowler D R and Miyazaki T 2010 Calculations for millions of atoms with density functional theory: linear scaling shows its potential *J. Phys.: Condens. Matter* **22** 074207
- [9] Prentice J C A, Aarons J, Womack J C, Allen A E A, Andrinopoulos L, Anton L, Bell R A, Bhandari A, Bramley G A, Charlton R J, Clements R J, Cole D J, Constantinescu G, Corsetti F, Dubois S M-M, Duff K K B, Escartín J M, Greco A, Hill Q, Lee L P, Linscott E, O'Regan D D, Phipps M J S, Ratcliff L E, Serrano Á R, Tait E W, Teobaldi G, Vitale V, Yeung N, Zuehlsdorff T J, Dziedzic J, Haynes P D, Hine N D M, Mostofi A A, Payne M C and Skylaris C-K 2020 The ONETEP linear-scaling density functional theory program *The Journal of Chemical Physics* **152** 174111
- [10] Bannwarth C, Ehlert S and Grimme S 2019 GFN2-xTB—An Accurate and Broadly Parametrized Self-Consistent Tight-Binding Quantum Chemical Method with Multipole Electrostatics and Density-Dependent Dispersion Contributions *J. Chem. Theory Comput.* **15** 1652–71
- [11] Aradi B, Hourahine B and Frauenheim Th 2007 DFTB+, a Sparse Matrix-Based Implementation of the DFTB Method *J. Phys. Chem. A* **111** 5678–84
- [12] Dolgonos G, Aradi B, Moreira N H and Frauenheim T 2010 An Improved Self-Consistent-Charge Density-Functional Tight-Binding (SCC-DFTB) Set of Parameters for Simulation of Bulk and Molecular Systems Involving Titanium *J. Chem. Theory Comput.* **6** 266–78
- [13] Dral P O, Wu X, Spörkel L, Koslowski A, Weber W, Steiger R, Scholten M and Thiel W 2016 Semiempirical Quantum-Chemical Orthogonalization-Corrected Methods: Theory, Implementation, and Parameters *J. Chem. Theory Comput.* **12** 1082–96
- [14] Akimov A V and Prezhdo O V 2015 Large-Scale Computations in Chemistry: A Bird's Eye View of a Vibrant Field *Chem. Rev.* **115** 5797–890
- [15] Grimme S, Bannwarth C and Shushkov P 2017 A Robust and Accurate Tight-Binding Quantum Chemical Method for Structures, Vibrational Frequencies, and Noncovalent Interactions of Large Molecular Systems Parametrized for All spd-Block Elements ($Z = 1-86$) *J. Chem. Theory Comput.* **13** 1989–2009
- [16] Budiutama G, Li R, Manzhos S and Ihara M 2023 Hybrid Density Functional Tight Binding (DFTB)—Molecular Mechanics Approach for a Low-Cost Expansion of DFTB Applicability *J. Chem. Theory Comput.* **19** 5189–98
- [17] Hohenberg P and Kohn W 1964 Inhomogeneous Electron Gas *Phys. Rev.* **136** B864–71
- [18] Kohn W, Becke A D and Parr R G 1996 Density Functional Theory of Electronic Structure *J. Phys. Chem.* **100** 12974–80
- [19] Chen M, Jiang X-W, Zhuang H, Wang L-W and Carter E A 2016 Petascale Orbital-Free Density Functional Theory Enabled by Small-Box Algorithms *J. Chem. Theory Comput.* **12** 2950–63
- [20] González D J and González L E 2009 Structure and motion at the liquid-vapor interface of some interalkali binary alloys: An orbital-free ab initio study *J. Chem. Phys.* **130** 114703
- [21] Carling K M and Carter E A 2003 Orbital-free density functional theory calculations of the properties of Al, Mg and Al–Mg crystalline phases *Modelling Simul. Mater. Sci. Eng.* **11** 339
- [22] Legrain F and Manzhos S 2015 Highly accurate local pseudopotentials of Li, Na, and Mg for orbital free density functional theory *Chem. Phys. Lett.* **622** 99–103
- [23] Huang C and Carter E A 2008 Transferable local pseudopotentials for magnesium, aluminum and silicon *Phys. Chem. Chem. Phys.* **10** 7109–20
- [24] Liu Q, Lu D and Chen M 2020 Structure and dynamics of warm dense aluminum: a molecular dynamics study with density functional theory and deep potential *J. Phys.: Condens. Matter* **32** 144002
- [25] Zhuang H, Chen M and Carter E A 2016 Elastic and Thermodynamic Properties of Complex Mg–Al Intermetallic Compounds via Orbital-Free Density Functional Theory *Phys. Rev. Applied* **5** 064021
- [26] Chai J-D, Lignères V L, Ho G, Carter E A and Weeks J D 2009 Orbital-free density functional theory: Linear scaling methods for kinetic potentials, and applications to solid Al and Si *Chem. Phys. Lett.* **473** 263–7
- [27] Koch D, Pavanello M, Shao X, Ihara M, Ayers P W, Matta C F, Jenkins S and Manzhos S 2024 The Analysis of Electron Densities: From Basics to Emergent Applications *Chem. Rev.* **124** 12661–737
- [28] Koch D and Manzhos S 2020 Oxygen Redox Activity in Cathodes: A Common Phenomenon Calling for Density-Based Descriptors *J. Phys. Chem. C* **124** 19962–8
- [29] Koch D, Chaker M, Ihara M and Manzhos S 2021 Density-Based Descriptors of Redox Reactions Involving Transition Metal Compounds as a Reality-Anchored Framework: A Perspective *Molecules* **26** 5541
- [30] Mi W, Luo K, Trickey S B and Pavanello M 2023 Orbital-Free Density Functional Theory: An Attractive Electronic Structure Method for Large-Scale First-Principles Simulations *Chem. Rev.* **123** 12039–104
- [31] Shao X, Jiang K, Mi W, Genova A and Pavanello M 2021 DFTpy: An efficient and object-oriented platform for orbital-free DFT simulations *WIREs Comput. Mol. Sci.* **11** e1482
- [32] Jiang K, Shao X and Pavanello M 2022 Efficient time-dependent orbital-free density functional theory: Semilocal adiabatic response *Phys. Rev. B* **106** 115153
- [33] Jiang K and Pavanello M 2021 Time-dependent orbital-free density functional theory: Background and Pauli kernel approximations *Phys. Rev. B* **103** 245102
- [34] Xu Q, Ma C, Mi W, Wang Y and Ma Y 2022 Nonlocal pseudopotential energy density functional for orbital-free density functional theory *Nat. Commun.* **13** 1385
- [35] Chi Y-C and Huang C 2024 High-Quality Local Pseudopotentials for Metals *J. Chem. Theory Comput.* **20** 3231–41
- [36] Mi W, Zhang S, Wang Y, Ma Y and Miao M 2016 First-principle optimal local pseudopotentials construction via optimized effective potential method *J. Chem. Phys.* **144** 134108

- [37] Chai J-D and Weeks J D 2007 Orbital-free density functional theory: Kinetic potentials and ab initio local pseudopotentials *Phys. Rev. B* **75** 205122
- [38] Lüder J and Manzhos S 2020 Nonparametric Local Pseudopotentials with Machine Learning: A Tin Pseudopotential Built Using Gaussian Process Regression *J. Phys. Chem. A* **124** 11111–24
- [39] Woo J, Kim H and Kim W Y 2022 Neural network-based pseudopotential: development of a transferable local pseudopotential *Phys. Chem. Chem. Phys.* **24** 20094–103
- [40] Chen M, Xia J, Huang C, Dieterich J M, Hung L, Shin I and Carter E A 2015 Introducing PROFESS 3.0: An advanced program for orbital-free density functional theory molecular dynamics simulations *Computer Physics Communications* **190** 228–30
- [41] Mi W, Shao X, Su C, Zhou Y, Zhang S, Li Q, Wang H, Zhang L, Miao M, Wang Y and Ma Y 2016 ATLAS: A real-space finite-difference implementation of orbital-free density functional theory *Computer Physics Communications* **200** 87–95
- [42] Li P, Liu X, Chen M, Lin P, Ren X, Lin L, Yang C and He L 2016 Large-scale *ab initio* simulations based on systematically improvable atomic basis *Computational Materials Science* **112** 503–17
- [43] Mortensen J J, Larsen A H, Kuisma M, Ivanov A V, Taghizadeh A, Peterson A, Haldrup A, Dohn A O, Schäfer C, Jónsson E Ö, Hermes E D, Nilsson F A, Kastlunger G, Levi G, Jónsson H, Häkkinen H, Fojt J, Kangsabanik J, Söderquist J, Lehtomäki J, Heske J, Enkovaara J, Winther K T, Dulak M, Melander M M, Ovesen M, Louhivuori M, Walter M, Gjerding M, Lopez-Acevedo O, Erhart P, Warmbier R, Würdemann R, Kaappa S, Latini S, Boland T M, Bligaard T, Skovhus T, Susi T, Maxson T, Rossi T, Chen X, Schmerwitz Y L A, Schiøtz J, Olsen T, Jacobsen K W and Thygesen K S 2024 GPAW: An open Python package for electronic structure calculations *The Journal of Chemical Physics* **160** 092503
- [44] Shao X, Mi W and Pavanello M 2021 Revised Huang-Carter nonlocal kinetic energy functional for semiconductors and their surfaces *Phys. Rev. B* **104** 045118
- [45] Mi W, Genova A and Pavanello M 2018 Nonlocal kinetic energy functionals by functional integration *The Journal of Chemical Physics* **148** 184107
- [46] Wang T, Luo K and Lu R 2024 Semilocal Kinetic Energy Density Functionals on Atoms and Diatoms *J. Chem. Theory Comput.* **20** 5176–87
- [47] Lehtomäki J and Lopez-Acevedo O 2019 Semilocal kinetic energy functionals with parameters from neutral atoms *Phys. Rev. B* **100** 165111
- [48] Constantin L A, Fabiano E and Della Sala F 2018 Semilocal Pauli–Gaussian Kinetic Functionals for Orbital-Free Density Functional Theory Calculations of Solids *J. Phys. Chem. Lett.* **9** 4385–90
- [49] Luo K, Karasiev V V and Trickey S B 2018 A simple generalized gradient approximation for the noninteracting kinetic energy density functional *Phys. Rev. B* **98** 041111
- [50] Snyder J C, Rupp M, Hansen K, Blooston L, Müller K-R and Burke K 2013 Orbital-free bond breaking via machine learning *J. Chem. Phys.* **139** 224104
- [51] Golub P and Manzhos S 2018 Kinetic energy densities based on the fourth order gradient expansion: performance in different classes of materials and improvement via machine learning *Phys. Chem. Chem. Phys.* **21** 378–95
- [52] Manzhos S and Golub P 2020 Data-driven kinetic energy density fitting for orbital-free DFT: Linear vs Gaussian process regression *J. Chem. Phys.* **153** 074104
- [53] Golub P and Manzhos S 2020 CONUNDrum: A program for orbital-free density functional theory calculations *Comput. Phys. Commun.* **256** 107365
- [54] Seino J, Kageyama R, Fujinami M, Iwabata Y and Nakai H 2019 Semi-local machine-learned kinetic energy density functional demonstrating smooth potential energy curves *Chem. Phys. Lett.* **734** 136732
- [55] Fujinami M, Kageyama R, Seino J, Iwabata Y and Nakai H 2020 Orbital-free density functional theory calculation applying semi-local machine-learned kinetic energy density functional and kinetic potential *Chem. Phys. Lett.* **748** 137358
- [56] Manzhos S 2020 Machine learning for the solution of the Schrödinger equation *Mach. Learn.: Sci. Technol.* **1** 013002
- [57] Yao K and Parkhill J 2016 Kinetic Energy of Hydrocarbons as a Function of Electron Density and Convolutional Neural Networks *J. Chem. Theory Comput.* **12** 1139–47
- [58] Kulik H, Hammerschmidt T, Schmidt J, Botti S, Marques M A L, Boley M, Scheffler M, Todorović M, Rinke P, Oses C, et al 2022 Roadmap on machine learning in electronic structure *Electron. Struct.*
- [59] Brockherde F, Vogt L, Li L, Tuckerman M E, Burke K and Müller K-R 2017 Bypassing the Kohn-Sham equations with machine learning *Nat. Commun.* **8** 872
- [60] Imoto F, Imada M and Oshiyama A 2021 Order-N orbital-free density-functional calculations with machine learning of functional derivatives for semiconductors and metals *Phys. Rev. Res.* **3** 033198
- [61] Meyer R, Weichselbaum M and Hauser A W 2020 Machine Learning Approaches toward Orbital-free Density Functional Theory: Simultaneous Training on the Kinetic Energy Density Functional and Its Functional Derivative *J. Chem. Theory Comput.* **16** 5685–94
- [62] Manzhos S, Lüder J and Ihara M 2023 Machine learning of kinetic energy densities with target and feature smoothing: Better results with fewer training data *J. Chem. Phys.* **159** 234115
- [63] Remme R, Kaczun T, Scheurer M, Dreuw A and Hamprecht F A 2023 KineticNet: Deep learning a transferable kinetic energy functional for orbital-free density functional theory *The Journal of Chemical Physics* **159** 144113
- [64] Zhang H, Liu S, You J, Liu C, Zheng S, Lu Z, Wang T, Zheng N and Shao B 2024 Overcoming the barrier of orbital-free density functional theory for molecular systems using deep learning *Nat Comput Sci* **4** 210–23
- [65] Hodges C H 1973 Quantum Corrections to the Thomas–Fermi Approximation—The Kirzhnits Method *Can. J. Phys.* **51** 1428–37
- [66] Fermi E 1928 Eine statistische Methode zur Bestimmung einiger Eigenschaften des Atoms und ihre Anwendung auf die Theorie des periodischen Systems der Elemente *Z. Physik* **48** 73–9

- [67] Lüder J, Ihara M and Manzhos S 2024 A machine-learned kinetic energy model for light weight metals and compounds of group III-V elements *Electron. Struct.* **6** 045002
- [68] Manzhos S 2024 <https://github.com/sergeimanzhos/GPRKE>
- [69] Unke O T and Meuwly M 2019 PhysNet: A neural network for predicting energies, forces, dipole moments, and partial charges *J. Chem. Theory Comput.* **15** 3678–93
- [70] Schütt K T, Sauceda H E, Kindermans P-J, Tkatchenko A and Müller K-R 2018 SchNet – A deep learning architecture for molecules and materials *J. Chem. Phys.* **148** 241722
- [71] Ghasemi S A, Hofstetter A, Saha S and Goedecker S 2015 Interatomic potentials for ionic systems with density functional accuracy based on charge densities obtained by a neural network *Phys. Rev. B* **92** 045131
- [72] Symons B C B, Bane M K and Popelier P L A 2021 DL_FFLUX: A Parallel, Quantum Chemical Topology Force Field *J. Chem. Theory Comput.* **17** 7043–55
- [73] Manzhos S and Ihara M 2023 Neural Network with Optimal Neuron Activation Functions Based on Additive Gaussian Process Regression *J. Phys. Chem. A* **127** 7823–35
- [74] Nukunodomanich M, Yoon H, Hyojae L, Kameda K, Ihara M and Manzhos S 2024 Machine learning of properties of lead-free perovskites with a neural network with additive kernel regression-based neuron activation functions *MRS Adv.*
- [75] Kameda K, Ariga T, Ito K, Ihara M and Manzhos S 2024 Machine learning the screening factor in the soft bond valence approach for rapid crystal structure estimation *Digital Discovery* **3** 1967–79
- [76] Manzhos S and Ihara M 2023 A controlled study of the effect of deviations from symmetry of the potential energy surface (PES) on the accuracy of the vibrational spectrum computed with collocation *The Journal of Chemical Physics* **159** 211103
- [77] Manzhos S and Ihara M 2023 Orders-of-coupling representation achieved with a single neural network with optimal neuron activation functions and without nonlinear parameter optimization *Artif. Intell. Chem.* **1** 100013
- [78] Manzhos S, Carrington T and Ihara M 2023 Orders of coupling representations as a versatile framework for machine learning from sparse data in high-dimensional spaces *Artif. Intell. Chem.* **1** 100008
- [79] Thant Y M, Wakamiya T, Nukunodomanich M, Kameda K, Ihara M and Manzhos S 2025 Kernel regression methods for prediction of materials properties: recent developments *Chem. Phys. Rev.*
- [80] Gonze X, Jollet F, Abreu Araujo F, Adams D, Amadon B, Applencourt T, Audouze C, Beuken J-M, Bieder J, Bokhanchuk A, Bousquet E, Bruneval F, Caliste D, Côté M, Dahm F, Da Pieve F, Delaveau M, Di Gennaro M, Dorado B, Espejo C, Geneste G, Genovese L, Gerossier A, Giantomassi M, Gillet Y, Hamann D R, He L, Jomard G, Laflamme Janssen J, Le Roux S, Levitt A, Lherbier A, Liu F, Lukačević I, Martin A, Martins C, Oliveira M J T, Poncé S, Pouillon Y, Rangel T, Rignanese G-M, Romero A H, Rousseau B, Rubel O, Shukri A A, Stankovski M, Torrent M, Van Setten M J, Van Troeye B, Verstraete M J, Waroquiers D, Wiktor J, Xu B, Zhou A and Zwanziger J W 2016 Recent developments in the ABINIT software package *Comput. Phys. Commun.* **205** 106–31
- [81] Perdew J P, Burke K and Ernzerhof M 1996 Generalized Gradient Approximation Made Simple *Phys. Rev. Lett.* **77** 3865–8
- [82] Manzhos S and Ihara M 2024 Degeneration of kernel regression with Matern kernels into low-order polynomial regression in high dimension *J. Chem. Phys.* **160** 021101
- [83] Manzhos S and Ihara M 2023 The loss of the property of locality of the kernel in high-dimensional Gaussian process regression on the example of the fitting of molecular potential energy surfaces *J. Chem. Phys.* **158** 044111
- [84] Sobol' I M 1967 On the distribution of points in a cube and the approximate evaluation of integrals *USSR Comput. Math. Math. Phys.* **7** 86–112
- [85] Duvenaud D, Nickisch H and Rasmussen C E 2011 Additive Gaussian Processes *Advances in Neural Information Processing Systems* 24 (NIPS 2011) pp 226–34
- [86] Manzhos S, Sasaki E and Ihara M 2022 Easy representation of multivariate functions with low-dimensional terms via Gaussian process regression kernel design: applications to machine learning of potential energy surfaces and kinetic energy densities from sparse data *Mach. Learn.: Sci. Technol.* **3** 01LT02
- [87] Hornik K 1991 Approximation capabilities of multilayer feedforward networks *Neural Networks* **4** 251–7
- [88] Scarselli F and Chung Tsoi A 1998 Universal Approximation Using Feedforward Neural Networks: A Survey of Some Existing Methods, and Some New Results *Neural Networks* **11** 15–37
- [89] Kůrková V 1992 Kolmogorov's theorem and multilayer neural networks *Neural Networks* **5** 501–6
- [90] Cybenko G 1989 Approximation by superpositions of a sigmoidal function *Math. Control Signal Systems* **2** 303–14
- [91] Funahashi K-I 1989 On the approximate realization of continuous mappings by neural networks *Neural Networks* **2** 183–92
- [92] Nees M 1994 Approximative versions of Kolmogorov's superposition theorem, proved constructively *Journal of Computational and Applied Mathematics* **54** 239–50
- [93] Hornik K, Stinchcombe M and White H 1990 Universal approximation of an unknown mapping and its derivatives using multilayer feedforward networks *Neural Networks* **3** 551–60
- [94] Katsura H and Sprecher D A 1994 Computational aspects of Kolmogorov's superposition theorem *Neural Networks* **7** 455–61
- [95] Sprecher D A 1996 A Numerical Implementation of Kolmogorov's Superpositions *Neural Networks* **9** 765–72
- [96] Sprecher D A 1997 A Numerical Implementation of Kolmogorov's Superpositions II *Neural Networks* **10** 447–57
- [97] Sprecher D A 1972 An improvement in the superposition theorem of Kolmogorov *Journal of Mathematical Analysis and Applications* **38** 208–13
- [98] Sprecher D A 1965 On the structure of continuous functions of several variables *American Mathematical Society* **115** 340–55
- [99] Sprecher D A 1993 A universal mapping for kolmogorov's superposition theorem *Neural Networks* **6** 1089–94

- [100] Sprecher D A and Draghici S 2002 Space-filling curves and Kolmogorov superposition-based neural networks *Neural Networks* **15** 57–67
- [101] Gorban A N 1998 Approximation of continuous functions of several variables by an arbitrary nonlinear continuous function of one variable, linear functions, and their superpositions *Applied Mathematics Letters* **11** 45–9
- [102] Bishop C M 2006 *Pattern Recognition and Machine Learning* (Singapore: Springer)
- [103] Goedecker S, Teter M and Hutter J 1996 Separable dual-space Gaussian pseudopotentials *Phys. Rev. B* **54** 1703–10
- [104] Rasmussen C E and Williams C K I 2006 *Gaussian Processes for Machine Learning* (Cambridge MA, USA: MIT Press)
- [105] Montavon G, Orr G B and Mueller K-R 2012 *Neural Networks: Tricks of the Trade* (Berlin Heidelberg: Springer)
- [106] Manzhos S and Carrington T 2021 Neural network potential energy surfaces for small molecules and reactions *Chem. Rev.* **121** 10187–217
- [107] Wu X H, Ren Z X and Zhao P W 2022 Nuclear energy density functionals from machine learning *Phys. Rev. C* **105** L031303
- [108] Nagai R, Akashi R and Sugino O 2020 Completing density functional theory by machine learning hidden messages from molecules *npj Comput Mater* **6** 1–8
- [109] Kasim M F and Vinko S M 2021 Learning the Exchange-Correlation Functional from Nature with Fully Differentiable Density Functional Theory *Phys. Rev. Lett.* **127** 126403
- [110] Nagai R, Akashi R and Sugino O 2022 Machine-learning-based exchange correlation functional with physical asymptotic constraints *Phys. Rev. Res.* **4** 013106
- [111] Wu J, Pun S-M, Zheng X and Chen G 2023 Construct exchange-correlation functional via machine learning *The Journal of Chemical Physics* **159** 090901
- [112] Dick S and Fernandez-Serra M 2020 Machine learning accurate exchange and correlation functionals of the electronic density *Nat Commun* **11** 3509